Journal of
Synchrotron Radiation

ISSN 0909-0495

Received 6 August 2007
Accepted 23 January 2008

X-ray crystallographic and biochemical characterizations of a mutant photosystem II complex from *Thermosynechococcus vulcanus* with the *psbTc* gene inactivated by an insertion mutation

Takahiro Henmi,[a] Masako Iwai,[b] Masahiko Ikeuchi,[c] Keisuke Kawakami,[d] Jian-Ren Shen[d] and Nobuo Kamiya[a]*

[a]Department of Chemistry, Graduate School of Science, Osaka City University, 3-3-138 Sugimoto, Sumiyoshi, Osaka 558-8585, Japan, [b]Department of Applied Biological Science, Faculty of Science and Technology, Tokyo University of Science, 2641 Yamazaki, Noda, Chiba 278-8510, Japan, [c]Department of Life Sciences (Biology), University of Tokyo, 3-8-1 Komaba, Meguro, Tokyo 153-8902, Japan, and [d]Division of Bioscience, Graduate School of Natural Science and Technology, Okayama University, 3-1-1 Tsushima-naka, Okayama 700-8530, Japan. E-mail: nkamiya@sci.osaka-cu.ac.jp

The crystal structure of a photosystem II (PSII) dimer from *Thermosynechococcus vulcanus* with its *psbTc* gene inactivated by insertion mutation of an antibiotic cassette in a site in the C-terminal region was analyzed at 3.8 Å resolution. In the crystal structure of the mutant PSII, the transmembrane helix of PsbTc remains, whereas the C-terminal loop of PsbTc has disappeared. In addition, the PsbM subunit, which seemed to be lost in a PsbTc-deletion mutant PSII of *T. elongatus*, is still present. The deletion of the C-terminal loop of PsbTc in the mutant PSII was verified by mass spectrometry. Thus, the insertion mutation of *psbTc* eliminated only the C-terminal loop of this subunit. Nevertheless, some features of the mutant PSII, namely a destabilization of the dimeric form and a slight decrease of the oxygen-evolving activity, were observed in the mutant, indicating that the C-terminal loop of PsbTc functions to maintain the stability of the PSII dimer and the activity of oxygen evolution.

Keywords: photosystem II; PsbTc; oxygen evolution; mutant; *Thermosynechococcus vulcanus*.

1. Introduction

Photosystem II (PSII) exists in the thylakoid membranes of oxygenic photosynthetic organisms and catalyzes light-induced water oxidation, leading to the evolution of molecular oxygen. PSII is a multisubunit pigment-protein complex containing a number of protein subunits, among which more than ten are so-called low-molecular-mass (LMM) subunits. Most of the LMM subunits have one transmembrane helix, with only one subunit having two helices (PsbZ). The structure of PSII has been reported at 3.8–3.0 Å resolution by X-ray crystallographic analysis of PSII isolated from thermophilic cyanobacteria (Zouni *et al.*, 2001; Kamiya & Shen, 2003; Ferreira *et al.*, 2004; Loll *et al.*, 2005). In the most recent structural model (Loll *et al.*, 2005), the locations of most of the LMM subunits have been assigned, although three transmembrane helices remain to be identified. The crystallographic studies, however, did not yield enough information on the functions of each of the LMM subunits.

PsbTc is one of the LMM subunits of PSII having a molecular mass of 4.7 kDa and is located in the monomer–monomer interface in the current PSII dimer structure. Analysis of a mutant of *Thermosynechococcus elongatus* lacking the *psbTc* gene suggested that PsbTc is involved in the dimerization of PSII and also possibly in the binding of PsbM, another LMM subunit located close to PsbTc, to the PSII complex (Iwai *et al.*, 2004). Recently, it was proposed that PsbTc affects the stability of the plastoquinone binding region of the D2 subunit from studies with a *Chlamydomonas* mutant lacking *psbTc* (Ohnishi *et al.*, 2007). In the present study, a mutant of *T. vulcanus*, whose *psbTc* gene was inactivated, was studied by means of X-ray crystallographic and biochemical analysis.

2. Experimental procedures

2.1. Construction of the mutant, and purification, crystallization of mutant PSII

The *psbTc* gene in *T. vulcanus* was inactivated by insertion of a chloramphenicol-resistant cassette with the same construction as used for the mutation of *T. elongatus* reported previously (Iwai *et al.*, 2004). Insertion of the cassette within *psbTc* was verified by PCR from genomic DNA of the mutant cells (data not shown). The mutant cells were grown in a liquid medium, and thylakoid membranes were prepared from the mutant cells by a combination of lysozyme-treatment and osmotic shock (Shen & Inoue, 1993). The thylakoid membranes were subsequently solubilized with lauryldimethylamine

N-oxide followed by differential centrifugation to obtain crude PSII particles. The crude PSII particles were finally solubilized with *n*-dodecyl-β-D-maltoside (DM) and purified with a Mono-Q anion exchange column (GE Healthcare UK Ltd). PSII monomer and dimer fractions from the anion exchange column were confirmed by a Superdex 200 gel filtration column (GE Healthcare UK Ltd) (Shen & Kamiya, 2000). The PSII dimer fraction was collected, precipitated by centrifugation after addition of PEG 1450 to a final concentration of 12.5%, and suspended in a solution containing 30 m*M* MES (pH 6.0), 20 m*M* NaCl and 3 m*M* $CaCl_2$.

Crystallization of mutant PSII dimer was performed with the hanging-drop method under conditions similar to those used previously for wild-type PSII (Shen & Kamiya, 2000; Kamiya & Shen, 2003). The crystals grew to a size larger than 400 × 300 × 200 µm during incubation at 293 K for two days.

2.2. Crystal structure analysis

The crystals were transferred to a cryoprotectant solution containing 25% glycerol and 20% PEG 1450 with a step-wise procedure and flash-cooled in a nitrogen gas stream at 100 K. X-ray diffraction data were collected with an X-ray wavelength of 0.9 Å at BL41XU (Kawamoto *et al.*, 2001) of SPring-8, Japan. The diffraction data were processed with *HKL-2000* (Otwinowski & Minor, 1997) and the electron density maps were calculated with *FFT* in the *CCP4* program suit (Collaborative Computational Project, Number 4, 1994) using the phase information obtained previously for wild-type PSII (Kamiya & Shen, 2003). The figure of PSII structure was constructed with *PyMOL* (DeLano, 2002).

2.3. Polyacrylamide gel electrophoresis (PAGE), mass spectrometry and oxygen evolution analysis

Sodium dodecylsulfate (SDS)/urea–PAGE was performed according to Ikeuchi & Inoue (1988) with slight modifications. A gradient gel containing 16–22% acrylamide with 6.5 *M* urea was used, and the samples were solubilized with 2.5% SDS. Tricine SDS–PAGE was performed according to Schägger & von Jagou (1987). Blue-native–PAGE was performed according to Schägger *et al.* (1994), Danielsson *et al.* (2006) and Wittig *et al.* (2006), with slight modifications (Kawakami *et al.*, 2007).

For mass spectrometric analysis, the PSII complex was separated by SDS/urea–PAGE, and polypeptides with molecular masses of 3000–5000 Da were eluted and analyzed by a Matrix-assisted laser desorption/ionization time-of-flight (MALDI–TOF) mass spectrometer (AXIMA-CFRplus, SHIMADZU/Kratos Co.). The resulting masses were assigned to their corresponding polypeptides on the basis of the calculated masses deduced from the gene sequences of *T. elongatus*.

Oxygen evolution was measured with a Clark-type oxygen electrode at 303 K under continuous saturating light with 1.0 m*M* phenyl-*p*-benzoquinone as electron acceptor.

3. Results and discussion

3.1. Purification of mutant PSII and analysis of its properties

The mutant cells with the *psbTc* gene inactivated by insertion of the antibiotic cassette grew at a rate comparable to that of the wild-type strain (data not shown). Fig. 1 shows the elution pattern of PSII from the final Mono-Q column of wild type and *psbTc*-inactivation mutant used in the present study. Three peaks appeared during the elution step (indicated as P1, P2 and P3 in Fig. 1), and it was

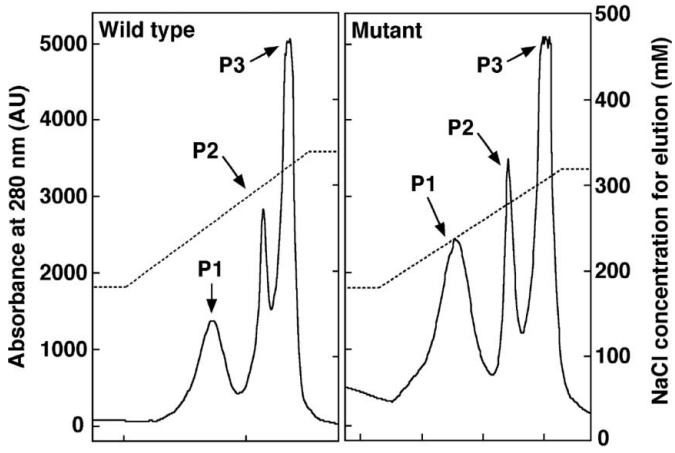

Figure 1
Elution profiles of PSII isolated from wild-type (left panel) and mutant (right panel) *T. vulcanus* from a Mono-Q anion exchange column (GE Healthcare UK Ltd). Absorbance at 280 nm is represented by a solid line and NaCl concentration for elution is indicated by a dashed line.

confirmed by gel filtration chromatography that these peaks were PSII monomer (P1), PSII dimer (P3) and a mixture of the two (P2). The ratio of PSII monomer to PSII dimer represented by the ratio of the peak area of P1 to that of P3 was larger in the mutant than in the wild type (Fig. 1), suggesting a destabilization of PSII dimer in the mutant. In order to confirm this, we analyzed the relative content of PSII dimer and monomer in the wild-type and mutant thylakoids by blue-native–PAGE, which can eliminate possible artifacts caused by detergent solubilization used for purification of PSII. The results are depicted in Fig. 2, which clearly shows that the content of PSII dimer was decreased whereas that of PSII monomer was increased in the mutant thylakoid membranes compared with those of the wild-type membranes. These results indicated that inactivation of the *psbTc* gene resulted in the destabilization of PSII dimer. We also analyzed the oxygen-evolving activity of crude PSII and purified PSII dimer from the mutant and wild-type cells, and found that the activity of mutant PSII was constantly lower than that of wild-type PSII by 10–30% (data not shown).

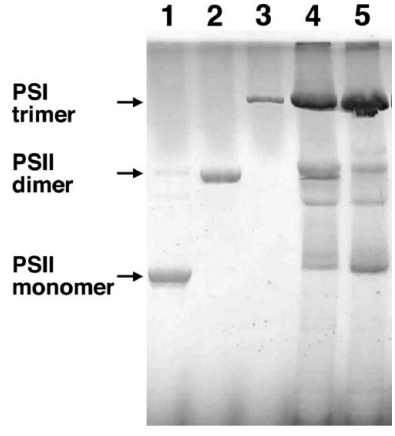

Figure 2
Blue-native–PAGE analysis of thylakoid membranes of the wild type and mutant. Lane 1, PSII monomer; lane 2, PSII dimer; lane 3, PSI trimer; lane 4, thylakoid membranes of wild type; and lane 5, thylakoid membranes of mutant. The amount of sample loaded was 0.8 µg of chlorophyll for lanes 1–3, and 15 µg of chlorophyll for lanes 4–5.

Table 1
Statistics of X-ray data collection.

Space group	$P2_12_12_1$
Unit-cell parameters (Å)	a = 129.0, b = 225.5, c = 306.3
Resolution (Å)	50.0–3.80
Completeness (%)	96.1 (80.5)†
$R_{\rm merge}$‡	0.083 (0.531)†
$I/\sigma(I)$	24.33 (2.43)†
Redundancy	6.4 (5.8)†
No. of unique reflections	85107

† The values in parentheses are for the highest-resolution shell (3.94–3.80 Å). ‡ $R_{\rm merge} = \Sigma_{hkl}\Sigma_i|I_{hkl,i} - \langle I_{hkl}\rangle|/\Sigma_{hkl}\Sigma_i I_{hkl,i}$, where I is the observed intensity and $\langle I\rangle$ is the average intensity for multiple measurements.

3.2. Crystal structure analysis of mutant PSII

The mutant PSII dimer could be crystallized with conditions similar to those used for crystallization of wild-type PSII dimer (Shen & Kamiya, 2000). X-ray diffraction data collected from the mutant crystals diffracted to a resolution of 3.8 Å (Table 1) and were highly isomorphous with those from the wild-type crystals (Kamiya & Shen, 2003). Using the previously obtained phase information, we were able to calculate the electron density maps of the mutant PSII crystal; the region corresponding to the transmembrane helix of PsbTc is shown in Fig. 3(*a*). It is clear that the electron densities corresponding to the transmembrane helix of PsbTc are still present in the mutant PSII, whereas the electron densities corresponding to the C-terminal loop of PsbTc have disappeared (Fig. 3*a*). This is supported by the difference Fourier map between wild-type and mutant PSII (Fig. 3*b*), in which a strong positive signal is observed around the C-terminal loop of PsbTc, whereas the electron densities corresponding to the transmembrane helix of PsbTc have disappeared. These results suggest that only the C-terminal loop of PsbTc is deleted and the transmembrane helix of PsbTc remains in the mutant PSII.

3.3. SDS–PAGE and mass spectrometric analysis of mutant PSII

In order to confirm the deletion of the C-terminal loop of PsbTc in the mutant PSII, we performed SDS–PAGE and mass spectrometric analysis. Fig. 4 compares the polypeptide composition of purified wild-type and mutant PSII dimer by (*a*) SDS/urea–PAGE and (*b*) tricine SDS–PAGE. The band corresponding to PsbTc in wild-type

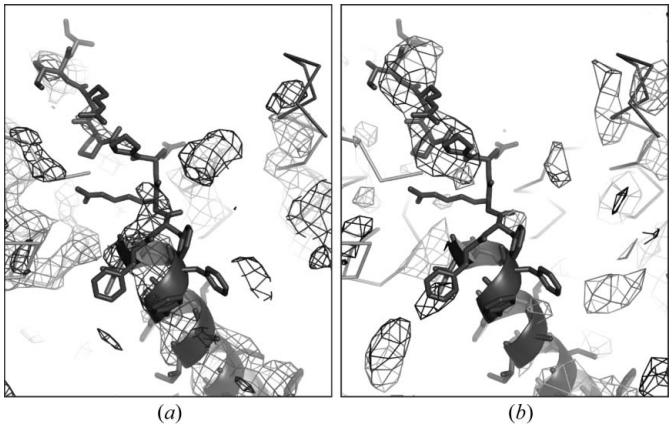

(*a*) (*b*)

Figure 3
Electron density map of the mutant PSII crystal (*a*) and a difference Fourier map of wild-type-minus-mutant PSII (*b*) around the transmembrane helix and its C-terminal loop of PsbTc. The electron density map (*a*) at a resolution of 3.8 Å is represented at 2.0σ. The difference Fourier map (*b*) is computed at a resolution of 6.0 Å and displayed at 2.0σ, where positive signals are represented by black mesh and negative signals are represented by a light-gray mesh. PsbTc is depicted by cartoon with side chain, and other subunits are depicted as ribbons.

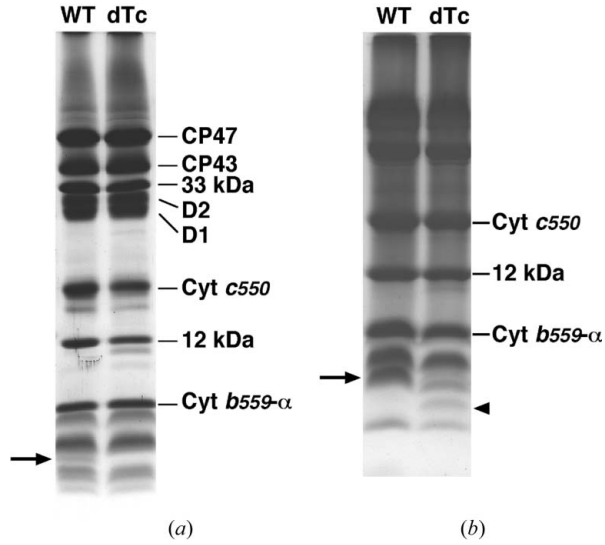

(*a*) (*b*)

Figure 4
SDS/urea–PAGE (*a*) and tricine SDS–PAGE (*b*) profiles of purified PSII dimer from wild type (left lane) and mutant (right lane). The subunit names are indicated on the right side of the panel. The arrows indicate the 4.7 kDa band corresponding to the PsbTc subunit. The arrowhead in (*b*) indicates the band corresponding to PsbTc lacking its C-terminal loop.

PSII [indicated by an arrow in Fig. 4(*a*)] disappears in the mutant PSII. When LMM subunits were further analyzed by tricine SDS–PAGE, however, a band with a slightly smaller molecular mass newly appeared in the mutant PSII, as indicated by an arrowhead in Fig. 4(*b*). These results agree with the loss of the C-terminal loop of PsbTc in the mutant. To further confirm these results, we analyzed the masses of polypeptides separated by SDS–PAGE in the range 3000–5000 Da from both wild-type and mutant PSII. The results show that a polypeptide with a molecular mass of 3904.5 was detected only in the wild-type PSII but not in the mutant PSII; the mass of this polypeptide corresponds to that of PsbTc whose N-terminal methionine is formylated. On the other hand, a molecular mass of 3011.2 was detected only in the mutant PSII, which corresponds to a fragment of PsbTc truncated at the site of the C-terminal loop where the antibiotic-resistant cassette was inserted. Thus, the mutant PSII analyzed in the present study has lost its C-terminal loop only.

In conclusion, we analyzed the crystal structure of PSII dimer from the mutant of *T. vulcanus* with its *psbTc* gene inactivated by insertion mutation at 3.8 Å resolution, and found that the PsbTc subunit lost its C-terminal loop but retained its transmembrane helix in the mutant PSII. SDS–PAGE and mass spectrometric analysis indicated that the molecular mass of the truncated PsbTc found in the mutant PSII matches that of the PsbTc fragment with its C-terminal loop lost from the insertion site of the chloramphenicol-resistant cassette, indicating that the insertion of the antibiotic-resistant cassette has induced an early termination of translation and consequently a deletion of the C-terminal loop of PsbTc. The deletion of the C-terminal loop of PsbTc induced a partial destabilization of the dimeric form of PSII, leading to an increase of PSII monomer. Additionally this mutation decreased the oxygen-evolving activity slightly. Since the C-terminal loop of PsbTc is close to the D2 reaction center subunit, and since it is suggested that PsbTc stabilizes the plastoquinone binding region of D2 (Ohnishi *et al.*, 2007), our results may suggest that the oxygen-evolving activity in the mutant PSII decreased as a consequence of a destabilization of the plastoquinone binding region of D2. The present results also raised cautions on the construction of mutants by insertion inactivation of the targeted gene, especially at a site close

to the C-terminal region, as this may still allow translation of the majority of the gene, leading to a truncated product instead of the loss of the whole gene product that was initially intended.

This work was supported by a Grant-in-Aid for Scientific Research on Priority Areas (Structures of Biological Macromolecular Assemblies) from the Ministry of Education, Culture, Sports, Science and Technology of Japan.

References

Collaborative Computational Project, Number 4 (1994). *Acta Cryst.* D**50**, 760–763.
Danielsson, R., Suorsa, M., Paakkarinen, V., Albertsson, P. A., Styring, S., Aro, E. M. & Mamedov, F. (2006). *J. Biol. Chem.* **281**, 14241–14249.
DeLano, W. L. (2002). *PyMOL*, http://pymol.sourceforge.net/.
Ferreira, K. N., Iverson, T. M., Maghlaoul, K., Barber, J. & Iwata, S. (2004). *Science*, **303**, 1831–1838.
Ikeuchi, M. & Inoue, Y. (1988). *Plant Cell Physiol.* **29**, 695–705.
Iwai, M., Katoh, H., Katayama, M. & Ikeuch, M. (2004). *Plant Cell Physiol.* **45**, 1809–1816.
Kamiya, N. & Shen, J.-R. (2003). *Proc. Natl Acad. Sci. USA*, **100**, 98–103.
Kawakami, K., Iwai, M., Ikeuchi, M., Kamiya, N. & Shen, J.-R. (2007). *FEBS Lett.* **581**, 4983–4987.
Kawamoto, M., Kawano, Y. & Kamiya, N. (2001). *Nucl. Instrum. Methods Phys. Res. A*, **467–468**, 1375–1379.
Loll, B., Keren, J., Saenger, W., Zouni, A. & Biesiadka, J. (2005). *Nature* (*London*), **438**, 1040–1044.
Ohnishi, N., Kashino, Y., Satoh, K., Ozawa, S. & Takahashi, Y. (2007). *J. Biol. Chem.* **282**, 7107–7115.
Otwinowski, Z. & Minor, M. (1997). *Methods Enzymol.* **276**, 307–326.
Schägger, H., Cramer, W. A. & von Jagou, G. (1994). *Anal. Biochem.* **217**, 220–230.
Schägger, H. & von Jagou, G. (1987). *Anal. Biochem.* **166**, 368–379.
Shen, J.-R. & Inoue, Y. (1993). *Biochemistry*, **37**, 1825–1832.
Shen, J.-R. & Kamiya, N. (2000). *Biochemistry*, **39**, 14739–14744.
Wittig, I., Braun, H. P. & Schägger, H. (2006). *Nat. Protoc.* **1**, 418–428.
Zouni, A., Witt, J.-T., Kern, J., Fromme, P., Kraub, N., Saenger, W. & Orth, P. (2001). *Nature* (*London*), **409**, 739–743.